SUPPORTING INFORMATION

Engineered 3D-Printed $Bi_4O_5I_2$@Hematite Scaffolds for Visible Light Photocatalytic Degradation of Cresols

Akash Rawat[a,⊤], Raphael B. de Oliveira[b,c,⊤], Tapas Pal[d], Kleuton A. L. Lima[c], Guilherme S. L. Fabris[c], Raphael M. Tromer[e], Marcelo L. Pereira Junior[b,f], Adarsh Singh[g], Ashok Kumar Gupta[g,], Douglas S. Galvão[c,*], Chandra Sekhar Tiwary[h,*]*

[a] School of Environmental Science and Engineering, Indian Institute of Technology Kharagpur, Kharagpur 721302, India.

[b] Materials Science and Nano Engineering Department, Rice University, Houston, TX, 77005, USA.

[c] Applied Physics Department and Center for Computational Engineering & Sciences, State University of Campinas, Campinas, São Paulo 13083-970, Brazil.

[d] School of Nanoscience and Technology, Indian Institute of Technology Kharagpur, Kharagpur 721302, India.

[e] University of Brasília, Institute of Physics, Brasilia 70910900, Federal District, Brazil.

[f] University of Brasília, College of Technology, Department of Electrical Engineering, Brasilia 70910900, Federal District, Brazil.

[g] Environmental Engineering Division, Department of Civil Engineering, Indian Institute of Technology Kharagpur, Kharagpur - 721302, India.

[h] Metallurgical and Materials Engineering, Indian Institute of Technology Kharagpur, Kharagpur - 721302, India.

**Corresponding authors (Email: agupta@civil.iitkgp.ac.in; chandra.tiwary@metal.iitkgp.ac.in; galvao@ifi.unicamp.br)*

[⊤]Equal contribution

S1. Materials and chemical reagents

Bismuth (III) nitrate pentahydrate ($Bi(NO_3)_3 \cdot 5H_2O$; ≥ 99% purity), Potassium iodide (KI; ≥ 99% purity), Ethylene glycol ($C_2H_6O_2$; ≥ 99% purity), Sodium hydroxide (NaOH; ≥ 99% purity, Hydrochloric acid (HCl; 35%), Ethanol (C_2H_5OH; ≥ 99.9%). Ascorbic acid ($C_6H_8O_6$; ≥ 99.9%), Silver nitrate ($AgNO_3$), and 2-propanol (C_3H_8O; ≥ 99.99% purity). Carboxymethyl cellulose (CMC, as binder). Cresol isomers used in this study: p-cresol (C_6H_5OH; ≥ 99% purity), o-cresol (C_6H_5OH; ≥ 99% purity), and m-cresol (C_6H_5OH; ≥ 99% purity). All of the chemicals were used in analytical grade without further purification and purchased from Merck India.

S2. Instrumentation and characterization

The surface morphology of specimens was analyzed using high-resolution field emission gun scanning electron microscopy (FEG-SEM: Zeis Merlin Gemini II). Malvern PANalytical X'Pert Powder recorded the X-ray diffraction (XRD) pattern of as-fabricated materials. Electron paramagnetic resonance (EPR) spectroscopy (Bruker Corporation ELEXSYS) detected the principal ROS released during photocatalysis. The leaching of Fe and Bi ions was measured by multi-elemental scans using inductively coupled plasma optical emission spectroscopy (ICP-OES: iCAP PRO, Thermo Scientific, USA). The intermediates of *p*-cresol after certain intervals were identified by liquid chromatography-tandem mass spectrometry (LC-MS/MS: WATERS 2695, USA).

The concentrations of cresols in suspension were analyzed using high-performance liquid chromatography (HPLC: Thermo Fisher Scientific, Ultimate 3000). A reverse-phase C18 column measuring 4.6 cm × 250 mm was employed. Total organic carbon (TOC) analyzer (TOC-L Series, Shimadzu, Japan), ion chromatography (IC: Dionex, ICS-2100, Thermo Scientific, USA), chemical oxygen demand (COD) digester (HACH, DRB200), and UV-Vis Spectrophotometer (Agilent Cary 60).

S3. Detailed experimental setup

Fig. S1a, shows the picture of a bench-top experimental setup used in this study for the photocatalytic degradation of cresols. This setup consists of several components, including a visible light source (Lumina 50 Watts LED, 6500 K cool daylight with a luminous flux of 105 lm/w), a hot plate magnetic stirrer (Tarsons digital spinnot), a jacketed beaker of 200 mL capacity, a 60-watt peristaltic pump (RAVEL, model no. RH-P1205), water recirculation chamber (referred to as WRC; of 1000 mL beaker). Moreover, the zoomed-in image of the photocatalytic reactor (Fig. S1b) unveils the other components, such as the hanging stainless steel frame for holding the $Bi_4O_5I_2$@3DH scaffold.

Fig. S1 illustrates the experimental setup, where an LED light was positioned 5 cm above the jacketed beaker. Inside the beaker, the $Bi_4O_5I_2$/3DH scaffold was placed on a stainless steel frame and immersed in the cresol solution. Water circulated through the outer jacket to provide cooling, maintaining the solution temperature at 25 ± 5 °C. Chilled water was pumped from the WRC through a dedicated bottom inlet, which filled the outer jacket and exited through a top outlet. The warmed water was then returned to the WRC for mixing and recirculation.

S4. Experimental procedure

During photocatalysis, 2 mL samples were collected and filtered using a PVDF 0.2 µm (Agilent) syringe filter. The filtered samples were then analyzed by HPLC to determine the concentrations of cresol isomers.

The mobile phase used in HPLC was a mixture of acetonitrile and DI water in a 60:40 (V/V) ratio, with a detection wavelength set at 272 nm. The flow rate was kept constant at 1 mL/min, allowing for the detection of *p*-cresol, *o*-cresol, and *m*-cresol at retention times of 4.2, 4.35, and 4.3 minutes, respectively. Moreover, the TOC removal and degradation efficiency were calculated using the procedure explained in our previous study. [12]

S5. DFT calculations

The interaction process and the electronic properties of the $Bi_4O_5I_2$/Hematite interface were investigated using Density Functional Theory with Hubbard correction (DFT+*U*),[3] as implemented in the Spanish Initiative for Electronic Simulations with Thousands of Atoms (SIESTA) code.[4,5] Exchange-correlation effects were treated within the Generalized Gradient Approximation using the Perdew-Burke-Ernzerhof functional,[6] combined with a double-ζ polarized basis set composed of numerical atomic orbitals. A mesh cutoff of 350 Ry was employed in all simulations. Structural optimizations were carried out until all residual atomic forces were below 0.05 eV/Å. A Monkhorst-Pack Γ-centered **k**-point mesh was used, with a 3×3×1 sampling for monolayers and 3×3×3 for bulk systems.[7] For systems containing Fe atoms, a Hubbard *U* value of 6.0 eV was applied to account for the on-site Coulomb interaction of localized 3d orbitals.[8]

Initially, we analyzed the bulk structures of hematite (Fig. S2a) and $Bi_4O_5I_2$ (Fig. S2b). The unit cells consist of 30 atoms for hematite and 44 atoms for $Bi_4O_5I_2$. To model the $Bi_4O_5I_2$/hematite interface, we created a 4×4×1 hematite supercell composed of 320 atoms (Fig. S2c). A (001) monolayer of hematite was selected due to its higher structural stability, as demonstrated in previous works.[9–11] A vacuum layer of 40 Å was added along the *z*-direction to prevent interactions between periodic images. The monolayer was treated as a substrate, with periodicity maintained along the *x* and *y* directions, reproducing the configuration commonly observed in experimental settings.

To simulate the deposition process, a flake of $Bi_4O_5I_2$ was positioned above the hematite monolayer. This flake was generated by removing the periodic boundary conditions from the $Bi_4O_5I_2$ unit cell, treating it as a discrete, non-periodic cluster. Its initial vertical position, approximately 3.5 Å above the substrate, was determined using the Adsorption Locator module

from the Materials Studio suite.[12] This method employs a Monte Carlo algorithm to generate and evaluate multiple initial configurations of the adsorbate on the surface. Each configuration is assessed using an empirical force field to estimate its potential energy, and the configuration with the lowest energy is selected as the most favorable adsorption site. This configuration was then used as the starting point for complete relaxation of the heterostructure. The final geometry obtained is consistent with trends reported in previous experimental studies.

S6. Plausible degradation pathways of *p*-cresol

As depicted in Fig. 7a, the photoinduced degradation of p-cresol follows a couple of tentative pathways, mainly driven by OH radicals. In the first path, p-cresol (m/z 108.5) is attacked on the ortho position, resulting in the aromatic ring hydroxylation, which may form 4-methyl catechol (m/z 124.03).[13] Parallelly, the second pathways start with the oxidation of the methyl group on the aromatic ring, leading to the formation of 3,4-Dihydroxybenzoic acid (m/z 155.4) via the formation of 4-Hydroxybenzyl alcohol (m/z 124.12)[13] and 4-Hydroxybenzaldehyde (m/z 122.1) after reacting with OH, which is further oxidized into 2,4-Dihydroxybenzaldehyde (m/z 138.12) and 4-Hydroxybenzoic acid (m/z 138.12).[13] Although 4-Hydroxybenzyl Alcohol, 4-Dihydroxybenzaldehyde (m/z 138.12)[14] and 4-Hydroxybenzoic[13] acid were not detected in this study, they were still included due to their significance reported in previous studies. Interestingly, both plausible pathways converge at the subsequent generation of 3,4-Dihydroxybenzoic acid (m/z 155.4), which further undergoes the ortho-cleavage pathway. Thereafter, it ends up with open rings moieties, such as 2-butanol (m/z 75), acrolein (m/z 56), glycerol (m/z 92), oxalic acid (m/z 90), acetic acid (m/z 61), fumaric acid (m/z 116), ethylene glycol (m/z 62), and glycolic acid (m/z 77), which are mineralized into CO2 and H2O.[1,2]

Table S1: Parameters used in DIW for the hematite grid printing.

Parameters	Value
Slice height	0.6 mm
Nozzle diameter	1.2 mm
Speed	1 mm/sec
Infill pattern	Grid
Infill density	50%
Temperature	Room Temperature

Table S2. The predicted results for the intermediate and degradation products (IDPs) of p-cresol with corresponding toxicity profiles.[15]

Parent compound or degradation product	Name and m/z ratio	Chemical structure	Predicted acute toxicity (mg/L)*		Binary endpoint toxicity measures[T]		
			Daphnia magna LC50 (48 h)	Fathead minnow LC50 (96 h)	Developmental toxicity	Mutagenicity	Bio-concentration
TP-0	p-Cresol (m/z 107)	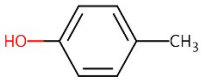	6.57	28.79	0.21	0.06	9.39
TP1[13]	4-Methyl catechol (m/z 123.04)	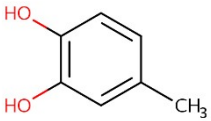	7.48	26.97	0.24	0.31	4.7
TP-2[13]	4-Hydroxyben zaldehyde (m/z 122)	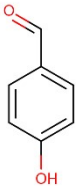	6.12	15.91	0.20	0.11	NA
TP-3[13]	4-Hydroxyben zyl Alcohol (m/z 124.14)	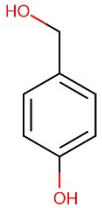	11.75	51.74	0.17	-0.12	3.75

TP-4[14]	2,4-Dihydroxybenzaldehyde (m/z 138.12)	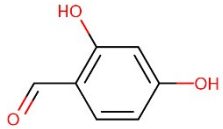	9.21	16.17	0.18	0.19	NA
TP-5[13]	4-Hydroxybenzoic acid (m/z 138)	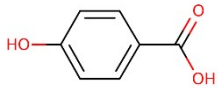	55.72	92.62	0.32	0.27	1.54
TP-6	3,4-Dihydroxybenzoic acid (m/z 155.4)	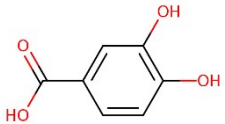	50.41	83.60	0.46	0.15	1.05
X1[1,2]	2-butanol (m/z 75)	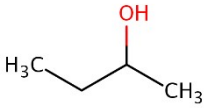	229.09	919.73	0.6	0.01	2.92
X2[1,2]	Acrolein (m/z 56)	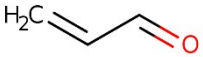	36.06	8.87	0.64	0.51	NA
X3[1,2]	Glycerol (m/z 92)	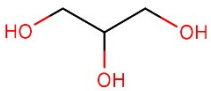	6304.90	10970.21	0.47	0.12	0.57

X4[1,2]	Oxalic acid (m/z 90)	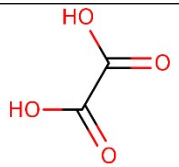	1445.45	702.23	0.56	0.30	0.17
X5[1,2]	Acetic acid (m/z 61)	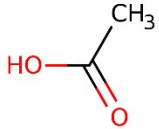	1035.97	762.37	0.71	-0.06	0.60
X6[1,2]	Fumaric acid (m/z 116),	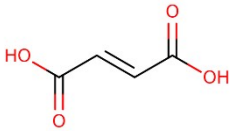	201.03	187.87	0.79	0.19	0.53
X7[1,2]	Ethylene glycol (m/z 62)	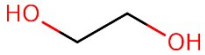	2898.89	5701.09	0.28	-0.03	0.74
X8[1,2]	Glycolic acid (m/z 77)	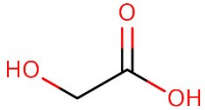	3323.98	2075.11	0.53	0.08	0.31

**Very Toxic (≤ 1 mg/L), Toxic (1–10 mg/L), Harmful (10–100 mg/L), and non-toxic (≥ 100 mg/L)*[16]

[1]if calculated score < 0.5, then activity = negative else if calculated score ≥ 0.5, then activity = positive[16]

Table S3. Physico-chemical characteristics of real water matrices.

Parameters	**DI water**	**Tap water**	**Pond water**	**Secondary treatment effluent**
pH	6.5 ± 2	7.2 ± 0.15	6.45 ± 0.3	6.7 ± 0.5
Turbidity (NTU)	BDL	0.65 ± 0.2	10.5 ± 0.3	25.5 ±2
TSS (mg/L)	BDL	5 ± 0.4	40 ± 0.5	55 ± 0.5
TDS (mg/L)	BDL	97 ± 5	150 ± 5	355 ± 5
Chloride (as Cl^-, mg/L)	BDL	5.5 ± 0.5	58.13 ± 2.5	75.2 ± 1
Sulfate (SO_4^{2-}, mg/L)	BDL	2.1 ± 0.5	23.8 ± 0.8	18.6 ± 0.5
Nitrate (NO_3^-, mg/L)	BDL	BDL	26.65 ± 4.5	75.23 ± 2.5
Phosphate (as PO_4^{3-}, mg/L)	BDL	BDL	10.3 ± 1	26.2 ± 0.2
COD (mg/L)	BDL	BDL	95 ± 5	72 ± 5

Table S4. Comparison of cresol photocatalytic degradation performance of $Bi_4O_5I_2$@3DH scaffold and other reported immobilized photocatalyst systems degrading phenolic compounds.

Photocatalyst system (Catalyst@Substrate)	**Catalyst**	**Substrate**	**Immobilization Method**	**Light source (Power)**	**Pollutant**	**Removal efficiency (Reaction time)**
TiO_2@Steel[17]	TiO_2	Steel	Sol-gel	365 nm UV-LED (400 W m^{-2})	Phenol (50 mg/L)	100% (3 h)
NiO/TiO_2@SSM[18]	NiO/TiO_2	Stainless steel (SSM)	Hydrothermal	254 nm UV-C (36 W)	Bisphenol A (10 mg/L)	96% (2 h)
BCI-CN-PPF[19]	$BiOCl_{0.75}I_{0.25}$/g-C_3N_4	Polyolefin polyester fiber (PPF)	Hydrothermal	420 nm Xenon lamp (500 W)	Bisphenol A (10 mg/L)	100% (1 h)
S-TiO_2@Glass[20]	S-TiO_2	Glass plate	Spray-coating	315 - 610 nm Visible light	Benzoic acid (20 mg/L)	41% (2 h)
CeO_2@Cellulose[21]	CeO_2	Cellulose acetate	Solution casting	375 nm Hg-Xe lamp (15 mW/cm^2)	4-nitrophenol (~ 14 mg/L mg/L)	97.7% (2.5 h)
rGO/ZrO_2/Ag_3PO_4@Glass[22]	rGO/ZrO_2/Ag_3PO_4	Glass	Spin coating	UV light	4-nitrophenol	92% (2.5 h)
TiO_2@Sand[23]	TiO_2	Sand	Epoxy coating	UV-A (60 W/m^2)	Phenol (25 mg/L)	50% (4 h)
Bi4O5I2@3DH *(Present study)*	**Bi4O5I2/hematite**	**3D printed hematite scaffold**	**Dip coating**	**Visible LED (50 W)**	***p*-cresol; *o*-cresol; *m*-cresol (20 mg/L)**	**99.78%; 99.80%; 99.23% (4 h)**

List of figures of ESI

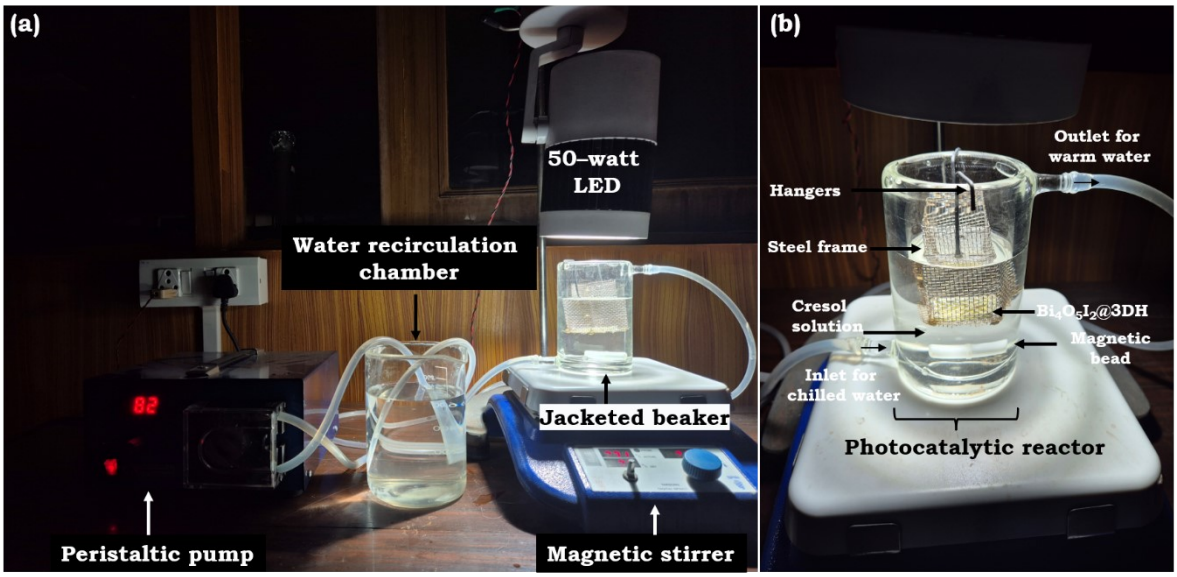

Fig. S1. (a) Bench-top photocatalytic experimental setup with water recirculation arrangement for maintaining the internal temperature of aqueous cresol solution. (b) Photocatalytic reactor highlighting its components.

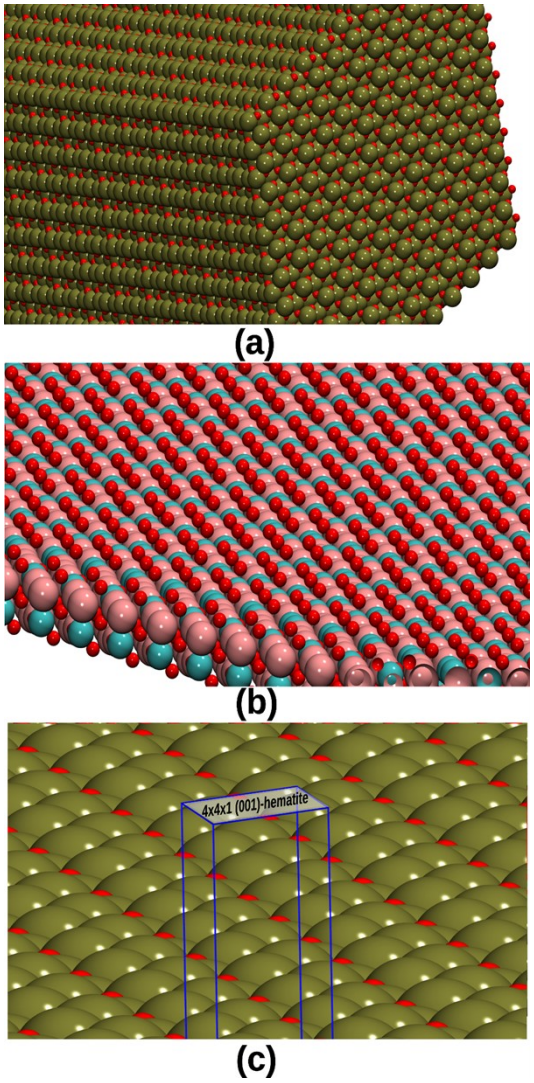

Fig. S2. Optimized structures: (a) bulk hematite, (b) bulk $Bi_4O_5I_2$, and (c) hematite (001) surface with the 4×4 supercell. Atomic species are colored as follows: red (O), blue (I), pink (Bi), and green (Fe).

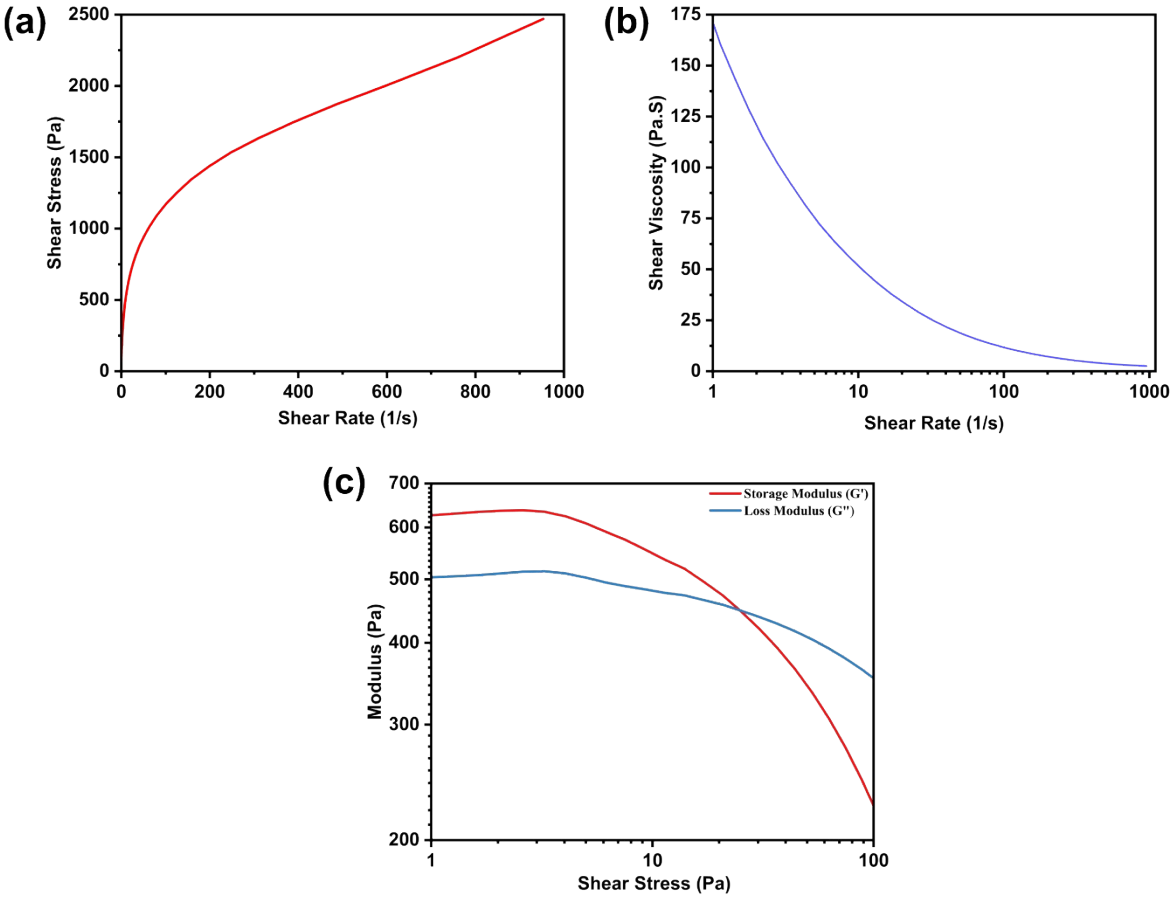

Fig. S3. Rheological Analysis of ink (a) Shear Stress vs Shear Rate, (b) Shear Viscosity vs Shear Rate, (c) Modulus vs Shear Stress.

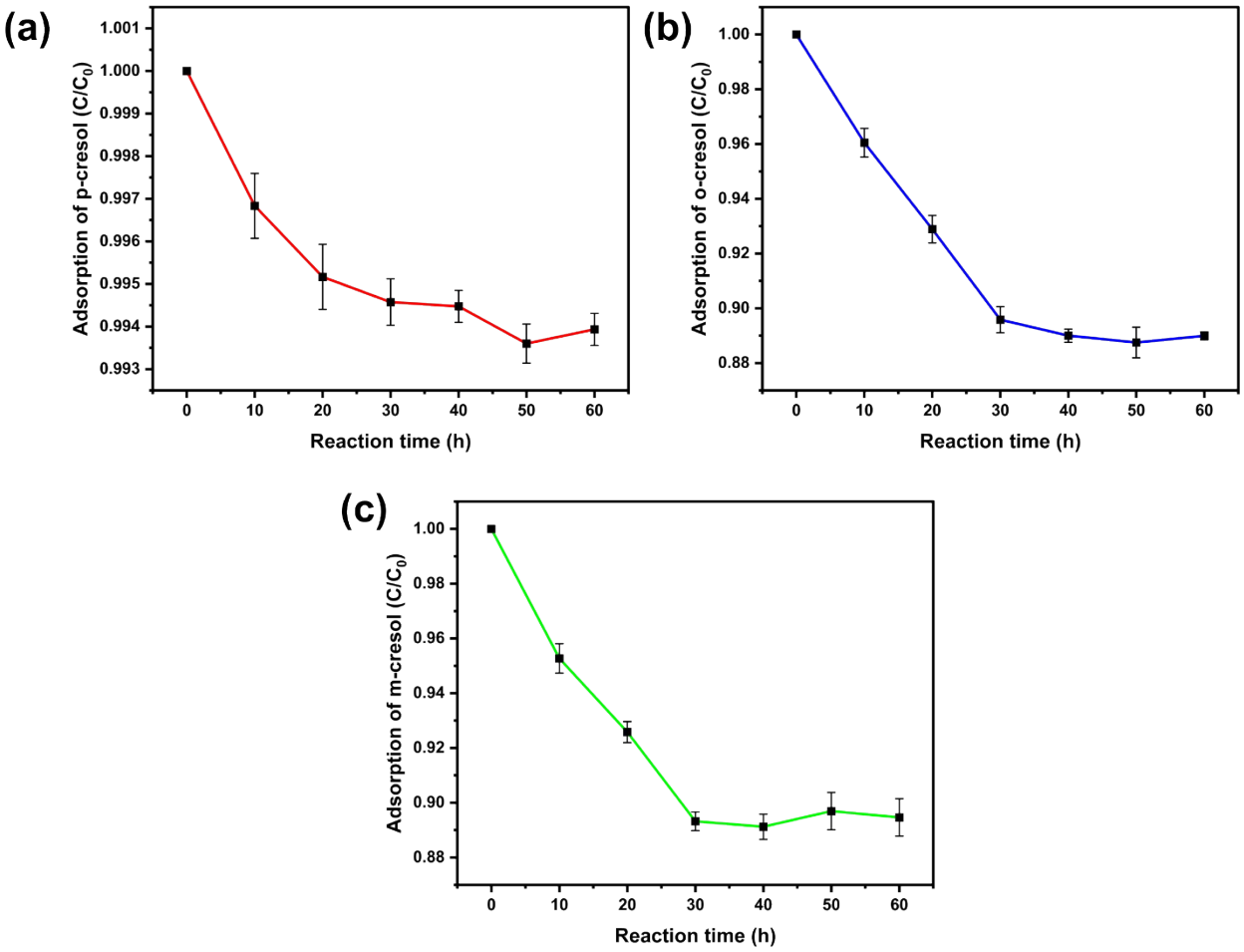

Fig. S4. Adsorption capacity of Bi4O5I2@3DH against the cresol isomers: (a) *p*-cresol, (b) *o*-cresol, and (c) *m*-cresol, conducted under the following operational parameters: cresol isomer concentration of 20 mg/L, infill density of 50%, five dip-coating cycles, and pH 6.5.

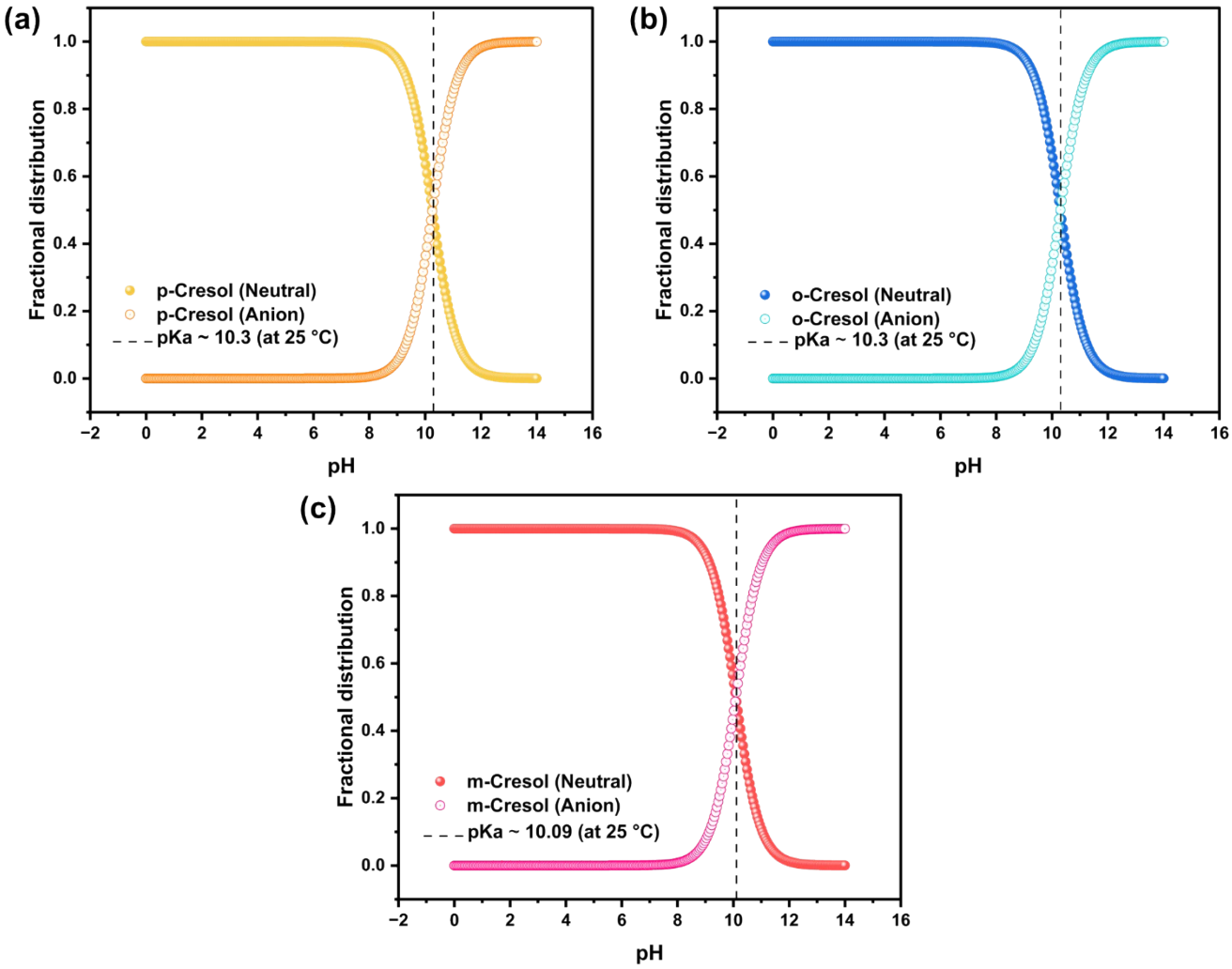

Fig. S5. Fractional distribution of cresol isomers at various pH: (a) *p*-cresol,[24,25] (b) *o*-cresol,[26,27] and (c) *m*-cresol.[26,28]

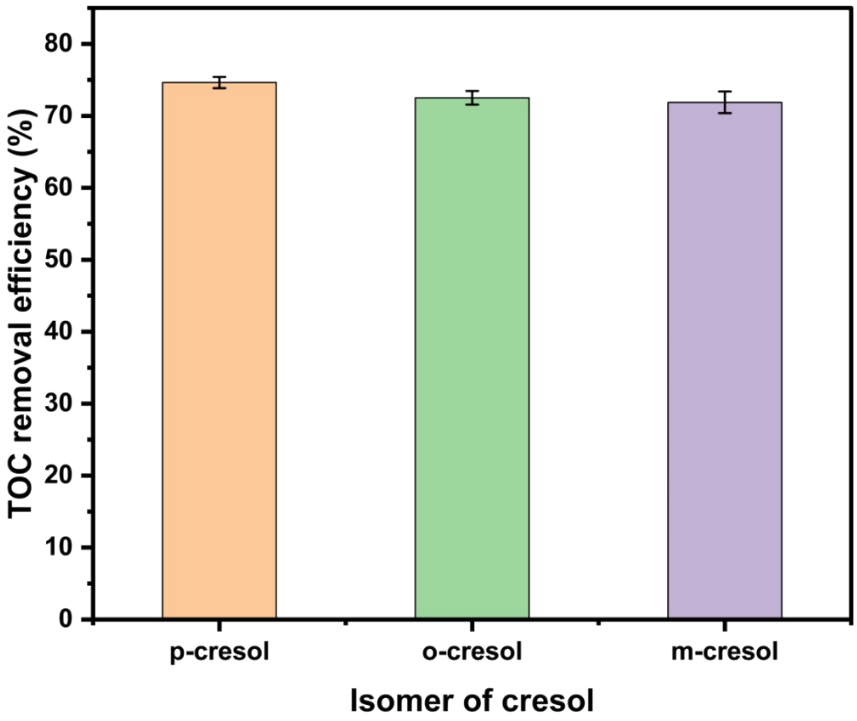

Fig. S6. TOC removal efficiency of individual cresol isomers (p-, o-, and m-cresol).

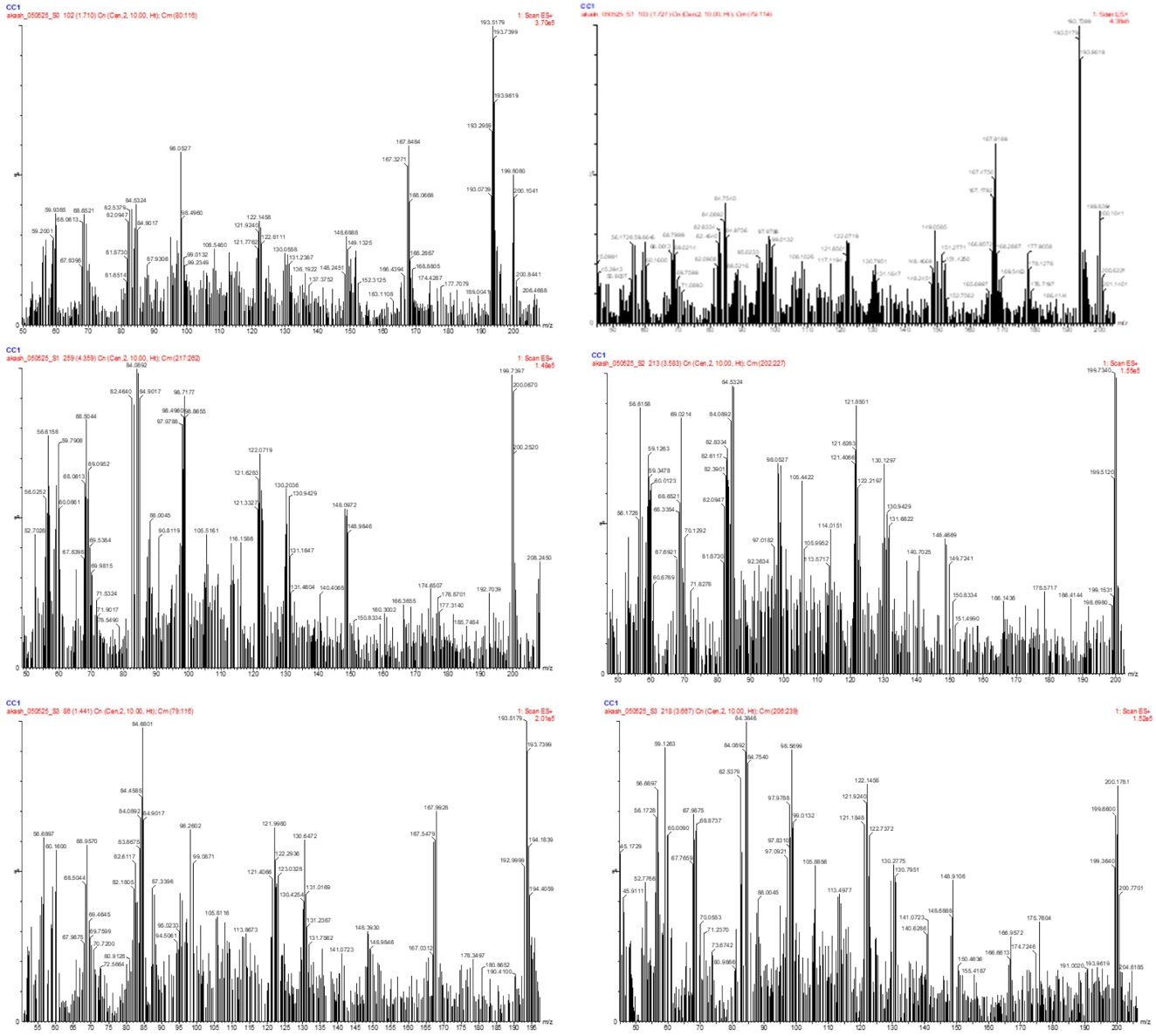

Fig. S7. The *m/z* spectra before and after the degradation of p-cresol: (i) sample extracted before photocatalysis, i.e., t = -30, (ii and iii) after one hour of photocatalysis, i.e., t = 60, (iv) t = 120, and (v and vi) after photocatalysis, i.e., t = 240 min.

References

1 A. Rawat, S. K. Srivastava, C. S. Tiwary and A. K. Gupta, *J. Mater. Chem. A*, 2025, **13**, 1271–1286.

2 A. Rawat, S. K. Srivastava, C. S. Tiwary and A. K. Gupta, *J. Environ. Chem. Eng.*, 2024, **12**, 112879.

3 W. Kohn and L. J. Sham, *Phys. Rev.*, 1965, **140**, A1133–A1138.

4 J. M. Soler, E. Artacho, J. D. Gale, A. García, J. Junquera, P. Ordejón and D. Sánchez-Portal, *J. Phys. Condens. Matter*, 2002, **14**, 2745–2779.

5 A. García, N. Papior, A. Akhtar, E. Artacho, V. Blum, E. Bosoni, P. Brandimarte, M. Brandbyge, J. I. Cerdá, F. Corsetti, R. Cuadrado, V. Dikan, J. Ferrer, J. Gale, P. García-Fernández, V. M. García-Suárez, S. García, G. Huhs, S. Illera, R. Korytár, P. Koval, I. Lebedeva, L. Lin, P. López-Tarifa, S. G. Mayo, S. Mohr, P. Ordejón, A. Postnikov, Y. Pouillon, M. Pruneda, R. Robles, D. Sánchez-Portal, J. M. Soler, R. Ullah, V. W. Yu and J. Junquera, *J. Chem. Phys.*, , DOI:10.1063/5.0005077.

6 J. P. Perdew, K. Burke and M. Ernzerhof, *Phys. Rev. Lett.*, 1996, **77**, 3865–3868.

7 H. J. Monkhorst and J. D. Pack, *Phys. Rev. B*, 1976, **13**, 5188–5192.

8 N. Naveas, R. Pulido, C. Marini, J. Hernández-Montelongo and M. M. Silván, *iScience*, 2023, **26**, 106033.

9 T. P. Trainor, A. M. Chaka, P. J. Eng, M. Newville, G. A. Waychunas, J. G. Catalano and G. E. Brown, *Surf. Sci.*, 2004, **573**, 204–224.

10 N. Dzade, A. Roldan and N. De Leeuw, *Minerals*, 2014, **4**, 89–115.

11 R. L. Blake, R. E. HessevicK, T. Zoltai and L. W. Finger, *Am. Mineral.*, 1966, **51**, 123–129.

12 D.S. Biovia, Material Studio, Dassault Systemes, https://www.3ds.com/products/biovia/materials-studio.

13 R. Khunphonoi and N. Grisdanurak, *Chem. Eng. J.*, 2016, **296**, 420–427.

14 Y. Ling, X. Fei, Q. Shan, D. Hei and W. Jia, *J. Radioanal. Nucl. Chem.*, 2018, **316**, 993–999.

15 E. CCTE, 2022.

16 GHS, *Globally Harmonized System of Classification and Labeling of Chemicals (GHS)*, 2021.

17 M. Schwarze, S. Borchardt, M. L. Frisch, J. Collis, C. Walter, P. W. Menezes, P. Strasser, M. Driess and M. Tasbihi, *Nanomaterials*, 2023, **13**, 1249.

18 N. Kim, M. Ali, H. Anwer, J.-W. Park and I. Irfan, *Chemosphere*, 2022, **308**, 136425.

19 Y. Qin, B. Yang, H. Li and J. Ma, *Sci. Total Environ.*, 2022, **842**, 156828.

20 L. Balassa, Á. Ágoston, Z. Kása, V. Hornok and L. Janovák, *J. Mol. Struct.*, 2022, **1260**, 132860.

21 V. Melinte, A.-L. Chibac-Scutaru, M. E. Culica and S. Coseri, *Appl. Surf. Sci.*, 2021, **565**, 150494.

22 H. Anwer and J.-W. Park, *J. Hazard. Mater.*, 2019, **369**, 375–383.

23 Y. K. Abdel-Maksoud, E. Imam and A. R. Ramadan, *Catal. Today*, 2018, **313**, 55–62.

24 National Center for Biotechnology Information, PubChem Compound Summary for CID 2879, P-Cresol, https://pubchem.ncbi.nlm.nih.gov/compound/P-Cresol.

25 P. J. Pearce and R. J. J. Simkins, *Can. J. Chem.*, 1968, **46**, 241–248.

26 W.-Y. Shiu, K.-C. Ma, D. Varhaníčková and D. Mackay, *Chemosphere*, 1994, **29**, 1155–1224.

27 National Center for Biotechnology Information (2025), PubChem Compound Summary for CID 335, O-Cresol, https://pubchem.ncbi.nlm.nih.gov/compound/O-Cresol.

28 National Center for Biotechnology Information (2025), PubChem Compound Summary for CID 342, M-Cresol, https://pubchem.ncbi.nlm.nih.gov/compound/M-Cresol.